Systems/Circuits

Rapid Input-Output Transformation between Local Field Potential and Spiking Activity during Sensation but not Action in the Superior Colliculus

Clara Bourrelly,[1,4] Corentin Massot,[1,2,4] and Neeraj J. Gandhi[1,3,4]
[1]Departments of Bioengineering, [2]Neurobiology, [3]Neuroscience, University of Pittsburgh, Pittsburgh, Pennsylvania 15213, and [4]Center for Neural Basis of Cognition, University of Pittsburgh, Pittsburgh, Pennsylvania 15213

Sensorimotor transformation is the sequential process of registering a sensory signal in the environment and then responding with the relevant movement at an appropriate time. For visually guided eye movements, neural signatures in the form of spiking activity of neurons have been extensively studied along the dorsoventral axis of the superior colliculus (SC). In contrast, the local field potential (LFP), which represents the putative input to a region, remains largely unexplored in the SC. We therefore compared amplitude levels and onset times of both spike bursts and LFP modulations recorded simultaneously with a laminar probe along the dorsoventral axis of SC in 3 male monkeys performing the visually guided delayed saccade task. Both signals displayed a gradual transition from sensory activity in the superficial layers to a predominantly motor response in the deeper layers, although the transition from principally sensory to mostly motor response occurred ~500 μm deeper for the LFP. For the sensory response, LFP modulation preceded spike burst onset by <5 ms in the superficial and intermediate layers and only when data were analyzed on a trial-by-trial basis. The motor burst in the spiking activity led LFP modulation by >25 ms in the deeper layers. The results reveal a fast and efficient input-output transformation between LFP modulation and spike burst in the visually responsive layers activity during sensation but not during action. The spiking pattern observed during the movement phase is likely dominated by intracollicular processing that is not captured in the LFP.

Key words: **frontal eye field; local field potential; oculomotor; saccade; superior colliculus**

Significance Statement

What is the sequence of events between local field potential (LFP) modulation and spiking activity during sensorimotor transformation? A trial-by-trial analysis reveals that the LFP activity leads the spike burst in the superficial and intermediate layers of the superior colliculus during visual processing, while both trial-by-trial and the average analyses show that the spike burst leads the LFP modulation during movement generation. These results suggest an almost instantaneous LFP input, spike burst output transformation in the visually responsive layers of the superior colliculus when registering the stimulus. In contrast, substantial intracollicular processing likely results in a saccade-related spike burst that leads LFP modulation.

Introduction

The orientation of gaze toward an object located in the visual field results from successions of neural processing that converts sensory information into movement generation. Located in the midbrain, the superior colliculus (SC) is an essential structure involved in this sensorimotor transformation (Sparks, 1986; Krauzlis, 2005; Gandhi and Katnani, 2011; Basso and May, 2017; Sajad et al., 2020; Cooper and McPeek, 2021). Studies using single-channel and multichannel electrodes have shown that the SC is functionally organized across its dorsoventral axis, such that its neurons modulate their activities in response to either stimulus appearance (superficial layers), saccade generation (deeper layers), or both (intermediate layers) (Mohler and Wurtz, 1976; Ikeda et al., 2015; Massot et al., 2019). The spikes emitted by neurons, identified after high-pass filtering and thresholding of the neural signal, are not the only signature of neural processing. The local field potential (LFP) present in the lower-frequency spectrum is also informative. Whereas the spikes are the output of neurons, the nature of the LFP is still debated and largely

Received Dec. 20, 2022; revised Apr. 19, 2023; accepted Apr. 21, 2023.

Author contributions: C.B., C.M., and N.J.G. designed research; C.B. and C.M. performed research; C.B. analyzed data; C.B. wrote the first draft of the paper; C.B., C.M., and N.J.G. edited the paper; C.B. and N.J.G. wrote the paper.

N.J.G. was supported by National Institutes of Health Grants R01 EY024831, R01 EY022854, and R21 EY030667. The work was also supported by National Institutes of Health Core Grant P30 EY08098 to the Department of Ophthalmology. We thank the Division of Laboratory Animal Resources for veterinarian care and surgical assistance.

The authors declare no competing financial interests.

Correspondence should be addressed to Neeraj J. Gandhi at neg8@pitt.edu or Clara Bourrelly at clb240@pitt.edu.

https://doi.org/10.1523/JNEUROSCI.2318-22.2023

unexplored in the SC (Chen and Hafed, 2018; Khademi et al., 2020). One hypothesis is that it represents the input and produces the spiking pattern observed in the neighboring neurons (Mitzdorf, 1985; Rasch et al., 2008; Buzsáki et al., 2012). Another possibility is that the LFP reflects the spiking activity occurring in a volume of tissue surrounding the recording contact (Zanos et al., 2011, 2012; Waldert et al., 2013). While it has been reported that LFP and spiking activities in SC share similar waveform profiles (Ikeda et al., 2015), it remains unclear from this single-electrode recording study whether the common features span the dorsoventral axis and for the entirety of the sensorimotor transformation process.

Previous studies have evaluated the relative timing of spike bursts and LFP modulations in the oculomotor system (Monosov et al., 2008; Ikeda et al., 2015; Sendhilnathan et al., 2017). In the frontal eye field (FEF), spatially nonselective modulation in the LFP precedes a burst of spikes in the visual epoch for various behavioral tasks, while the burst of spikes leads LFP modulation during saccade generation (Monosov et al., 2008; Sendhilnathan et al., 2017). These results suggest that the LFP could represent the synchronized input coming into the FEF. Since FEF neurons share similar properties with SC neurons, we sought to also study the timing of LFP and spiking activity in the SC during a visuomotor transformation. Favoring the hypothesis that visual information must arrive in the SC to activate its network, we expected LFP modulation to lead the visual spike burst, particularly in the superficial layers, although previous work indicate otherwise (Ikeda et al., 2015). Given that the SC operates with cortical oculomotor regions as an integrated network (Wurtz et al., 2001), we predicted the movement-related spike burst to lead LFP modulations. As a corollary, we also expected the two signals to display similar temporal dynamics during responses dominated by visual processes and not as much during saccade generation.

Using a laminar probe inserted approximately orthogonally to the SC surface, we recorded simultaneously spiking and LFP activities along the dorsoventral axis of SC while monkeys performed a visually guided delayed saccade task that temporally dissociates the visual and movement responses. We found that the LFP activity exhibits a systematic pattern across depth that is comparable to the trend observed in spiking activity, particularly during sensation. In the context of the input-output transformation, we analyzed the relative timing between the onsets of LFP modulation and spike burst during both visual and the motor epochs. Recognizing that single-trial and trial averaging analyses could lead to different results because averaging can alter the timing of abrupt changes in signals (Stokes and Spaak, 2016), we performed both types of analyses. We found that LFP modulation leads the onset of visual spike bursts in the visually responsive layers, although the lead time is very small and statistically significant only for analysis of individual trials. During the motor epoch, the motor burst strongly leads the LFP onset for deeper layers for both analyses. Together, these results are informative about spatial and temporal processes in the SC during sensorimotor transformation.

Materials and Methods

Animal preparation. All experimental and surgical procedures were approved by the Institutional Animal Care and Use Committee of the University of Pittsburgh and were in accordance with the guidelines of the U.S. Public Health Service policy on the humane care and use of laboratory animals. Three male rhesus macaque monkeys [*Macaca mulatta*, ages 8 (Monkey BL), 13 (Monkey BB), and 15 (Monkey SU) years] participated in the study. The details of the surgical procedures have been described previously (Katnani and Gandhi, 2011; Massot et al., 2019). To orthogonally access the left and right SCs, a recording chamber (tilted 40° posterior in the sagittal plane) was implanted on each animal. If needed, the penetration angle was adjusted by using a 3D printed angular adaptor.

Behavioral paradigm and data analysis. Training on eye movement tasks was done after recovery from surgical procedures. Stimulus display, behavioral paradigms, and all data acquisition were managed with a real-time LabView-based controller interface (Bryant and Gandhi, 2005). An LED-backlit flat screen television (120 frames/s, 1080p resolution) was used to present 4×4 white pixels on a dark gray background. The stimulus subtended ~0.5° of visual angle. The head was restrained by using a thermoplastic mask (Drucker et al., 2015). Eye position was sampled at 1 kHz with an infrared eye tracker (EyeLink 1000, SR Research) calibrated at the beginning of each session by having the animal fixate targets presented at known locations on the monitor.

Each trial of the visually guided delayed saccade task started with the appearance of a fixation target at the center of the screen. The monkey had 3000 ms to direct its line of sight on the central stimulus. Following a brief fixation period (200-350 ms for Monkeys BB and BL; 300 ms for Monkey SU), another target appeared in the visual periphery, but the animal had to keep its line of sight on the central target. After a span of 500-1150 ms ("delay period"), the central fixation target disappeared, which served as the "go cue" to produce a saccade to the peripheral stimulus. The eye position had to come close to the target (2°-4° radius window centered on the peripheral target but could have been extended depending on the calibration and the eccentricity of the stimulus) within ~600 ms, and the animal had to fixate this target for at least 250 ms to receive the reward (drop of water). All behavioral trials were analyzed offline using a custom-made software program. The onset and offset of the horizontal and vertical saccade components were detected based on a velocity threshold (30°/s). Every trial was also visually inspected, and the detected onset and offset were manually adjusted if deemed necessary.

Neurophysiological recordings and microstimulation. Neural activity across the dorsoventral axis of the SC was recorded with a laminar probe. A hydraulic Microdrive (Narishige) was used to drive a 16-channel laminar probe (Alpha-Omega; 150 μm intercontact distance; ~300 μm diameter; ~1 MΩ impedance for each channel) in Monkeys BB and BL or a 24-channel laminar probe (S-probe, Plexon; 200 μm intercontact distance; ~210 μm diameter) in Monkey SU. Once the probe was positioned in the intermediate layer of SC, its location was fine-tuned until multiunit activity could be detected on a qualitatively assessed, large number of contacts (i.e., channels). Electrical stimulation (40 μA, 400 Hz, 200 ms; biphasic, 200 μs pulse duration, 17 μs interpulse duration) was delivered individually on some channels, and the movements evoked on these contacts were averaged. The mean saccade vector (direction and amplitude) was used as an estimate of the preferred response field for all units recorded along the different contacts. The diametrically opposite vector was defined as the antireceptive field position. Target position was randomly interleaved between the preferred and antipreferred target locations. In this study, we only analyzed data from trials with the target at or near the response field center. At the end of each session, stimulation protocol was repeated systematically on each channel and behavior was recorded (for more details, see Katnani and Gandhi, 2011; Massot et al., 2019).

Neural data collection and processing. Neurophysiological signals were recorded using the Scout data acquisition system (Ripple). Neural data collection was synchronized with our LabView-based acquisition system at the beginning of every trial. The raw neural data on each channel were further filtered to isolate the LFP (low pass filter at 250 Hz) from the high-frequency activity (high pass filter at 250 Hz), which was then passed through a standard threshold crossing (threshold at 3.5 times the root mean square) to determine spike times. As it was impossible to isolate single-neural activity simultaneously on every channel, the recorded spikes were considered as multiunit activity. We did not

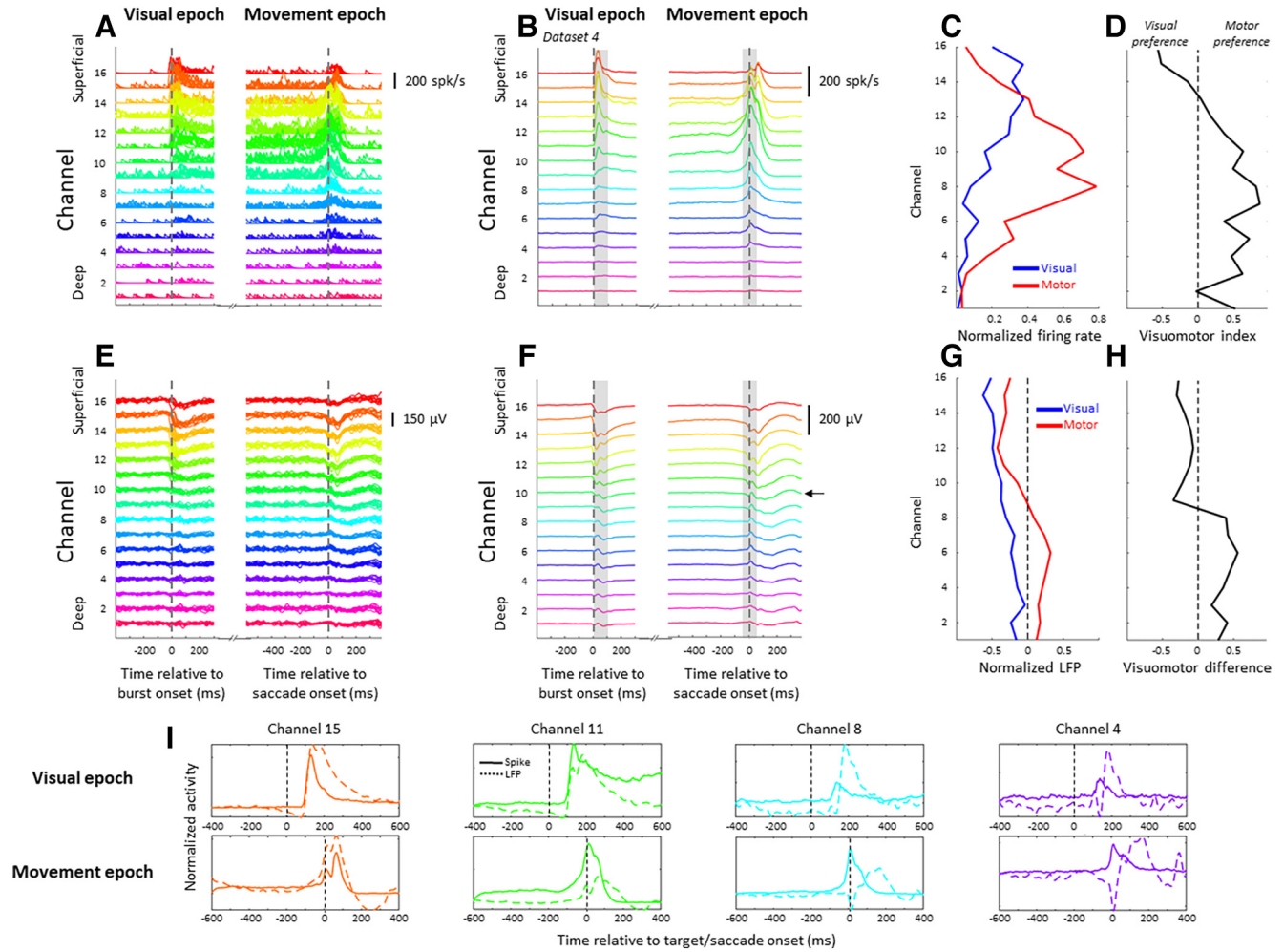

Figure 1. Signatures of sensation and action recorded with a laminar probe along the dorsoventral axis of the SC. ***A***, Plot of spike density traces of 10 example trials for each channel, aligned on burst (left) and saccade (right) onsets ($t = 0$ ms) for a representative session. Vertical dashed lines indicate visual burst onset and saccade onset times. The traces on each contact are shifted vertically for visualization. The method for aligning on burst onset is described in Materials and Methods. For this dataset, channel 15 was the "time alignment channel." ***B***, Plot of average spike density waveforms across all trials from the same session, using the same convention used in ***A***. Average firing rates in the shaded gray areas were used in ***C*** to quantify visual and motor activities. ***C***, The normalized average firing rates during the visual (blue line) and movement (red line) epochs are plotted as a function of depth. ***D***, The VMI is plotted as a function of depth. Negative and positive VMI values denote greater visual- and movement-related activities, respectively. Vertical dashed line indicates VMI = 0, or equal activities in both epochs. ***E***, Plot of LFP traces of the same 10 example trials used in ***A***. ***F***, Plot of average LFP traces across all trials, using the same convention used in ***A***. Shaded gray areas represent the epochs analyzed in ***G***. Arrow indicates the "reference channel" determined from the CSD analysis presented in Figure 2. ***G***, The normalized average LFP activity during the visual (blue line) and movement (red line) epochs is plotted as a function of depth for the same session. ***H***, The VMD is plotted as a function of depth. Negative and positive VMD values denote greater visual- and movement-related activities, respectively. Vertical dashed line indicates VMD = 0. ***I***, Plots of across-trials averages of normalized spiking and LFP activity recorded in visual (top row) and motor (bottom row) epochs, for four different channels from the same session. The colors match the channels in panels above. Spike density and LFP signals are shown as solid and dashed traces, respectively. The LFP signals are inverted (only in ***I***) to facilitate comparison with spiking activity on the same contact. The LFP is not a filtered representation of the underlying spiking activity.

attempt to perform spike sorting because we found in a previous study that spike sorting does not change the outcome of our analyses (Jagadisan and Gandhi, 2022). Continuous spike density waveforms (see examples in Figs. 1*A*,*B*,*I*, 4*A*,*C*) were obtained by convolving the spike trains with a kernel simulating an excitatory postsynaptic potential (growth and decay times constants of 1 and 20 ms, respectively) (Thompson et al., 1996). LFP activity (see examples in Figs. 1*E*,*F*,*I*, and 4*B*,*D*) was bandpass filtered between 0.7 and 30 Hz, although we also repeated our analyses with other cutoff frequencies (10 and 100 Hz; see Fig. 8). All data analyses were performed in MATLAB. Together, 35 sessions were recorded but only 32 were included in the analyses, as 3 exhibited noisy LFP signals or poor signal-to-noise ratio across all recording contacts.

Depth alignment of multiple sessions. Our analyses focus on neural activities across SC layers within a session and then averaging the data across sessions. This requires a procedure to spatially "shift" datasets so that all sessions are referenced to the same SC layer. We used an objective a method based on similarity of the features in the current source density (CSD) representation (Maier et al., 2011; Godlove et al., 2014; Zhao et al., 2014; Nandy et al., 2017; Massot et al., 2019). CSD is the second spatial derivative of LFP and provides an estimate of the distribution of the current sinks and sources as a function of space and time in a volume of tissue (Nicholson and Freeman, 1975; Pettersen et al., 2006). We calculated the CSD of normalized, trial-averaged, LFP signals separately for the visual [–400:600] ms relative to target onset) and motor [–600:400] ms relative to saccade onset) epochs. We normalized the LFP signal by dividing each value by the maximum absolute value observed across channels and trials within each epoch. If a channel was missing (i.e., channels 6 and 15 in Fig. 2*B*,*I*), we performed a linear interpolation between the two adjacent channels. We used the iCSD method in the csdplotter toolbox (https://github.com/espenhgn/CSDplotter) to generate the CSD (for data aligned on target and saccade onsets from an example dataset, see Fig. 2*A*,*F*). In the visual epoch data, a salient but not always consistent feature was a strong sink signal after target onset (see Fig. 2*A*; five datasets are shown in Fig. 2*C*). For each dataset, the channel closest to this "hotspot" was called the "reference channel" and assigned

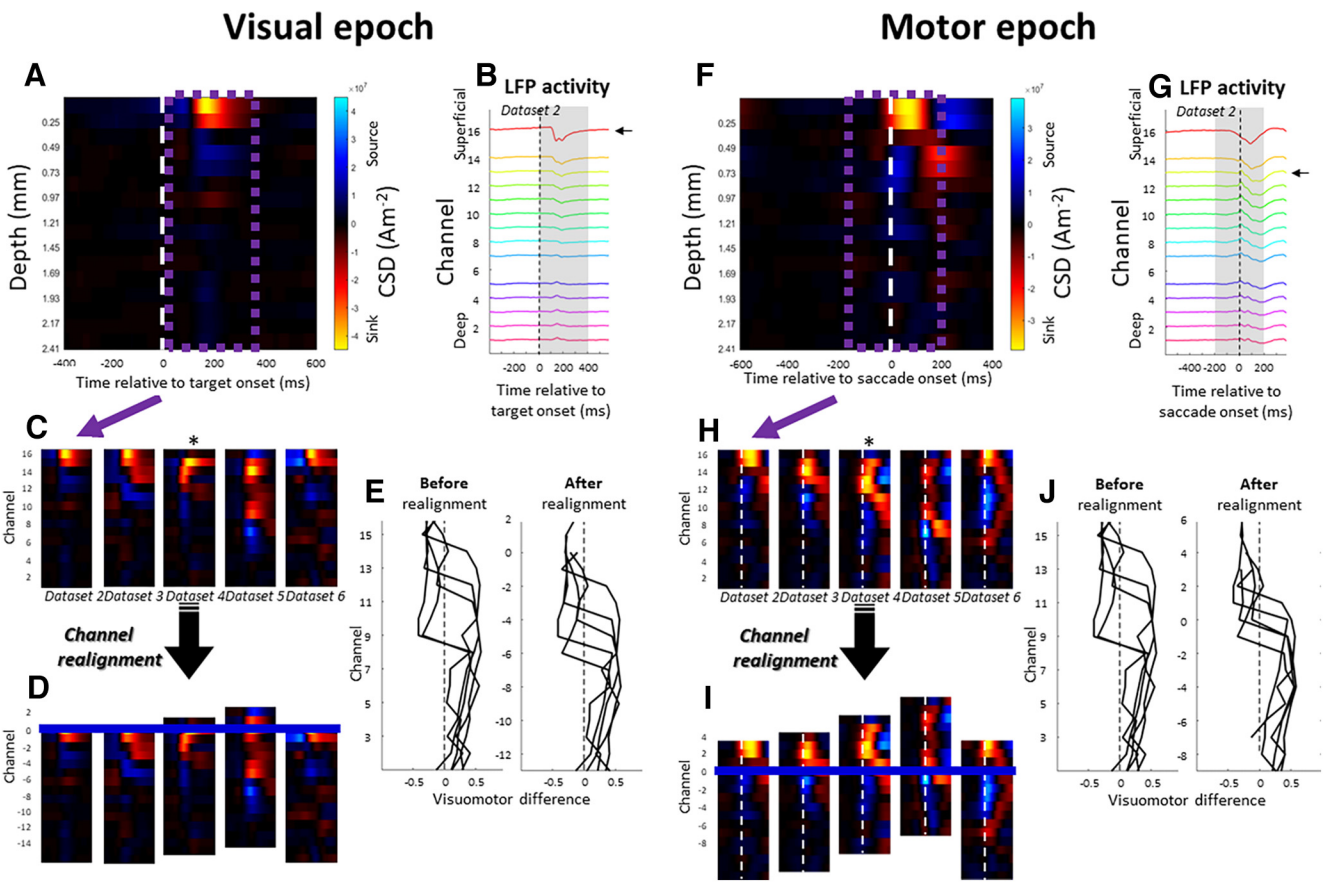

Figure 2. Alignment method using CSD computed on the visual and motor epochs. ***A***, CSD plot obtained from the LFP signals in ***B*** (see Materials and Methods) during the visual epoch. Positive and negative values correspond to current sources and sinks, respectively. Purple dashed square represents the CSD snippet in ***C*** indicated by the purple arrow. ***B***, Normalized LFP average activity across depth aligned on target onset for an example session. Black arrow indicates the reference channel (where the hotspot occurred). ***C***, Snippets of CSD (200 ms window around target onset) plots obtained from five different datasets before realignment. We identified a sink (i.e., hotspot) on channels 16, 16, 15, 14, and 16 (reference channels) in order from the left to right. ***C***, Middle, *Snippet of the CSD constructed from LFPs shown in Figure 1*F* (left). ***D***, Same five datasets as in ***C*** shifted to align with their reference channels, denoted by the blue horizontal line. ***E***, VMD of the same five datasets before (left) and after (right) realignment. ***A***, Vertical, dotted white line indicates target onset. ***F***, CSD plot obtained from the LFP signals in ***G*** (see Materials and Methods) during the motor epoch. Positive and negative values correspond to current sources and sinks, respectively. Purple dashed square represents the CSD snippet in ***H*** indicated by the purple arrow. ***G***, Normalized LFP average activity across depth aligned on saccade onset for an example session. Black arrow indicates the reference channel where the reversal occurred in the CSD plot. ***H***, Snippets of CSD (200 ms window around saccade onset) plots obtained from five different datasets before realignment. Note the sharp transition between sink and source currents on channels 13, 12, 10, 8, and 13 (reference channels) in order from the left to right. ***H***, Middle, *Snippet of the CSD constructed from LFPs shown in Figure 1*F* (right). ***I***, The five datasets shown in ***H*** are shifted to align with their reference channels, denoted by the blue horizontal line. ***J***, VMD of the same five datasets before (left) and after (right) realignment. ***F***, ***H***, ***I***, Vertical, dotted white lines indicate saccade onset. Channels 6 and 15 were unreliable waveform and therefore interpolated from adjacent channels before applying the CSD algorithm.

a depth of 0 in plots showing postalignment data (see Fig. 2*D*). The depths of all channels were shifted and expressed in term of distance (μm) with respect to the reference channel. The reference channel tended to be toward the superficial channels in our datasets. For the motor epoch, a more consistent pattern was found across datasets. The CSD analysis highlighted a sharp reversal between sink (red) and source (blue) currents around saccade onset (see Fig. 2*F*; additional datasets are shown in Fig. 2*H*). The channel closest to the locus of reversal was selected by visual inspection initially (later verified objectively by using the depth of CSD zero-crossing) was denoted as the reference channel and used for alignment. The CSD results revealed that the transition from sink to source occurred in the intermediate layer during the motor epoch (see Fig. 2*I*). Both alignment epochs yielded similar findings, as appreciated by the similarities of the postalignment distributions of visuomotor difference (see Fig. 2*E*,*J*). Given this similarity, we only report results based on alignment referenced to the reversal of CSD in the motor epoch, although we verified that similar outcomes were observed when relying on the visual epoch. Given that the intercontact distance of the probe was either 150 or 200 μm, the maximum error of alignment based on channel index can be 75 or 100 μm, respectively.

Initial analysis of neural activity. The study of visual activity, equivalently the neural response to stimulus presentation, is traditionally performed by aligning the data on target onset. This approach does not account for the trial-to-trial time variability in either the neuronal response (because of the stochastic nature of spiking activity) or the actual target presentation time. In the latter case, even after using, for example, a photodiode to identify and account for the frame in which the target is presented, there is still temporal uncertainty within a frame. We were concerned that these factors may produce variability larger than the time it takes for signals to propagate along the dorsoventral axis of SC. Therefore, we decided to analyze the visual response by aligning all data on spiking burst onset, as done previously (Massot et al., 2019). For each trial and channel, the "Poisson surprise" method (Hanes et al., 1995) was applied to the discrete spike train to detect burst onset in the epoch [50:250] ms following target onset. Burst detection criteria were set to a minimum of three spikes and a surprise index of –log(0.025). For each session, the channel with the maximum number of trials with detected bursts was selected as the "time alignment channel." The "time alignment channel" need not be the "reference channel" used for depth alignment across sessions (see above). Trials for which no burst onset was detected on the time alignment channel were discarded from the analyses associated with the visual epoch (~10% of the trials). For every remaining trial, the visual spike burst onset on the "time alignment channel" was used to align the activity on all the other channels. The

spike burst onset times of the time alignment channel were also used to align LFP data.

Neuronal activity categorization. Neurons in the SC can be classified depending on their activity during the visual and perisaccadic movement epochs. We performed analyses to determine how these features vary with depth. We worked with data already realigned on visual burst onset, which means our analysis was limited to trials in which a visual burst was detected on the "time alignment channel" but not necessarily every channel (see above). Also, we normalized the spiking and LFP signals by dividing the individual value of each trial by the maximum absolute value observed across channels and trials during the visual epoch. We then averaged the individual trials to get the normalized average spiking and LFP activity.

We computed the standard visuo-movement index (VMI) that contrasts the normalized visual and movement activities of multiunit spiking activity during saccade tasks. The visual activity (V) is the baseline-corrected average activity in the epoch [0:100] ms following visual burst onset. The movement activity (M) is the baseline-corrected average activity in the peri-saccadic epoch [−25:25] ms centered on saccade onset. Average baseline activities for the visual and motor epochs were computed, respectively, from the [−150:50] ms before the burst onset and [−300: −200] ms preceding the saccade onset. We defined the index as $VMI = (M - V)/(M + V)$; thus, VMI = −1 corresponds to a visual spiking activity with no saccade-related activity, while VMI = +1 corresponds to a movement-related activity with no visual response (as done previously in Massot et al., 2019). A different index was used to quantify LFP activity because, unlike spiking activity, LFP can be positive or negative. We introduced the so-called visuo-movement difference (VMD) measure to contrast the normalized LFP activity in visual and movement epochs. The visual activity (V) and the movement activity (M) were baseline-corrected and computed using the same epochs and conventions applied to the spiking data. We defined the index as $VMD = (M - V) \times \text{sign}(M)$. Thus, $VMD < 0$ implies a larger modulation in the visual period, while $VMD > 0$ denotes a bigger change in the movement window. Additionally, VMI and VMD were calculated on trial-averaged activities. If we had determined the indices on individual trials and then computed the average, we would obtain the same result given the linearity of this operation.

We also computed the conventional d' metric (Khanna et al., 2019) for both the spiking and the LFP activity. It is quantified as the difference in the means of the visual and motor activities divided by the product of their SDs. As for VMI and VMD, negative values of d' correspond to higher modulation in the visual window, while positive values denote a bigger modulation in the motor epoch.

Modulation onset analysis on trial-by-trial activity. The detection of the onset of spike burst and LFP modulation on each trial and each channel during both the visual and motor epochs was computed as follows (see Fig. 4). First, we obtained for each channel the trial-averaged spiking and LFP activities. This provided estimates of the times of the peak spiking activity and the troughs in LFP modulations in each epoch. These values were then used to define the actual temporal windows of analysis on individual trials to obtain precise onset times. For each channel and trial, the peak in spiking activity and trough in LFP waveform were detected in the epoch ∼[−30:50] ms around the peak and trough times obtained from the average traces. Importantly, the peak and trough activities had to be at least 2-3 SDs greater or lower than the mean baseline activity, respectively (see Fig. 4, green rectangles). If not, the trial was discarded from further analysis. The baseline measures were calculated [−350: −150] ms before burst onset (see Fig. 4*A*,*B*, green areas) and [−500: −200] ms before saccade onset (not shown). Because individual LFP traces are rather noisy, we increased the detection threshold to 3 SDs instead of 2 SDs (as it was used for spiking activities) to minimize false onset detection. Next, we performed a continuous piecewise linear fit on a 150-200 ms snippet of spike density or LFP activities that ended at the time of the peak or the trough (see Fig. 4, dashed blue lines within the shaded gray region). The time at which the two linear segments meet (inflection or hinge point) marked the onset of modulation. We excluded from our analysis all the onset times detected 50 ms after or 100 ms before the visual burst or saccade onset. We were able to detect a peak in 42% and 45% of the spike density waveforms and a trough in 24% and 21% of LFP traces during the visual and the motor epochs, respectively. We discuss this point in detail when presenting Figure 9.

Modulation onset analysis of across-trials average activity. The spike density waveforms and the LFP signals on each channel were averaged across trials. As above, the peak in each spike density trace and trough in each LFP signal were detected in an epoch ∼[−20:150] ms around the visual burst onset time and [−50:200] ms around the saccade onset time (see Fig. 4*C*,*D*, black crosses marking the end of the shaded area). It is important to keep in mind that the burst onset time refers to the realignment timing based on the Poisson surprise method (described above); it is not relative to target onset. As before, we constrained the peak and trough activities to be at least 2 SDs greater or lower than the mean baseline activity (see Fig. 4*C*,*D*, green areas). If not, the waveform was discarded from the analysis. We then performed a continuous piecewise linear fit (red dashed lines) on a 100-300 ms snippet of spike or LFP signals that ended at the time of the average peak or trough. The time of inflection (or hinge) point indicated the onset of modulation. We discarded the results with onset times detected 50 ms after and 100 ms before the visual burst or saccade onset. For a fair comparison, the average activity is based only on trials and channels used for the trial-by-trial analysis. For this reason, it is important to appreciate that the average spike density waveforms and LFPs used for the VMI and VMD analyses are not the same trials as the averages used to determine the onset of the average spiking and LFP modulations. Therefore, we also separately repeated the same analysis based on "global" average activity across all trials (see Fig. 7).

Relative timing. The relative timing is the difference between the onsets of the LFP modulation and the spiking burst. The individual onset values are the hinge points of the continuous piecewise linear regressions applied to the spike density and LFP profiles. A negative relative time value means that the LFP modulation starts before the neuron emits a burst of spikes, and a positive value means that the cell bursts before the LFP signal exhibits modulation. We computed this parameter for each channel on both individual trials and across-trials average. The relative timing can only be computed if modulations were detected on both spike density and LFP signals. Factors that contributed to an absence of detection include an actual lack of modulation or that the data were too noisy. Recall that we set the criteria to be very restrictive to avoid false detection because of noise in the trial-by-trial traces (especially in the LFP signal). Thus, we also repeated an average onset detection analysis on all trials (for details, see Fig. 7).

Statistics and reproducibility. A Kolomogorov–Smirnov test was used to assess the normality of the data distributions. We performed a parametric *t* test when the hypothesis of normality was not rejected. For the relative timing analysis, one-sample *t* test without correction was first applied. Because the LFP signal is not independent across depth, we also used two correction methods: one-sample *t* test at every 150 µm (approximate channel spacing) with Bonferroni correction and one-sample *t* test at each depth using the Benjamini–Hochberg procedure for reducing the false discovery rate (see Figs. 5*E*,*F*, 6*E*,*F*). Statistical significance threshold was set to $p < 0.05$ before correcting for multiple comparisons. To assess the goodness of the piecewise linear fit used to detect the modulation onsets, we computed the coefficient of determination (R^2; see Figs. 5*B*,*D*, 6*B*,*D*). To know at which depth the VMI and VMD switched from visual to motor activity (i.e., crossing point), we used the bootstrap method (see Fig. 3*B*–*E*), which was motivated by the fact that multiple crossing points were observed in both the VMI and VMD traces for individual sessions. We obtained VMI and VMD profiles for 1000 iterations performed with 100% of the data selected randomly with replacement (not shown) and then performed a two-sample *t* test.

Results

We performed a comparative analysis of bursts in spiking activity and modulations in LFP signals in the SC of monkeys performing the visually guided delayed saccade task. The use of laminar probes enabled an assessment of how these features in

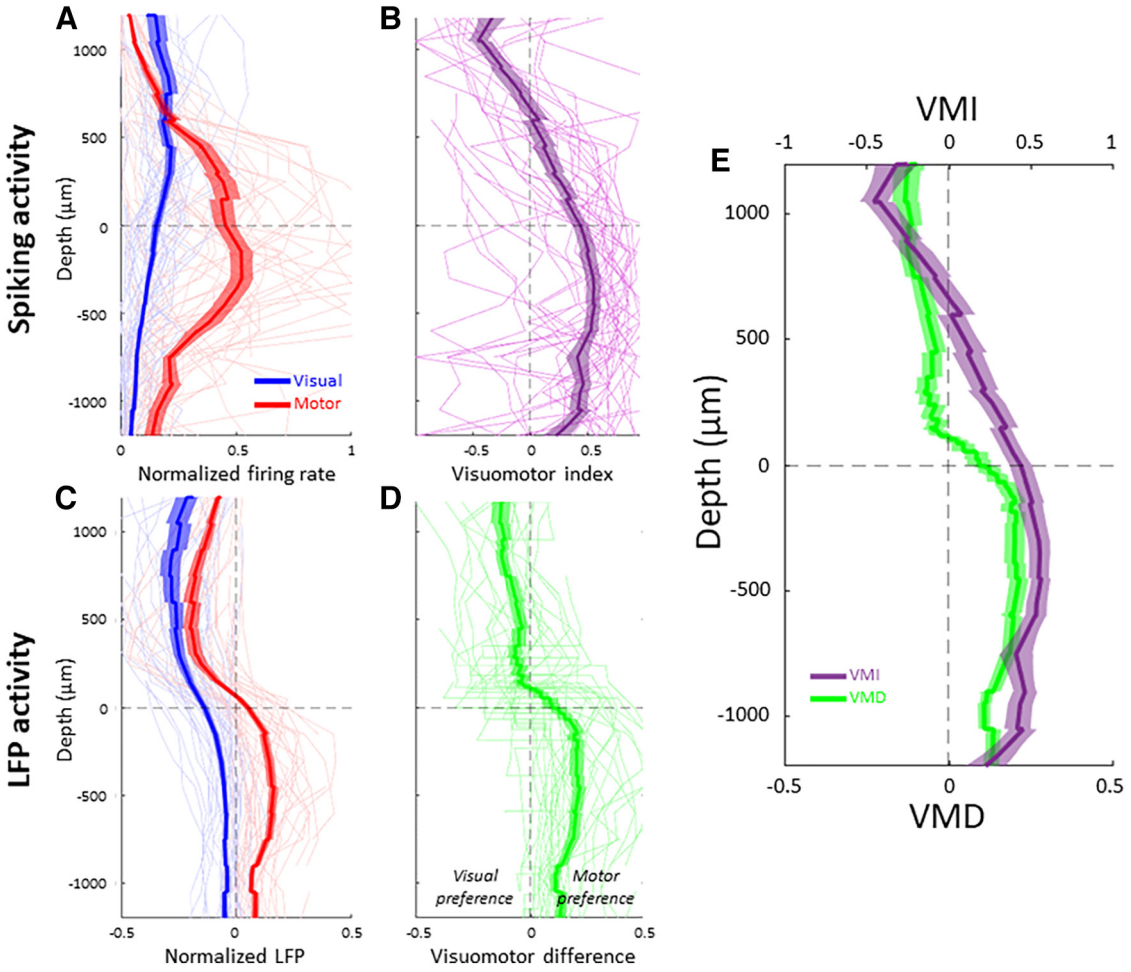

Figure 3. Spiking and LFP activity along the dorsoventral axis of SC. Data aligned on CSD of motor epoch. ***A***, The normalized firing rate averaged across sessions during the visual (thick blue trace) and movement (thick red trace) epochs are plotted as a function of depth after realignment based on the CSD of the motor epoch. Thin blue and red traces represent the normalized firing rates in the two epochs for individual sessions. Each channel's reference channel is positioned at zero depth. ***B***, The session-averaged VMI is plotted as a function of depth (thick purple trace). Thin purple traces represent the VMI for individual datasets. ***C***, The normalized LFP activity averaged across sessions during the visual (thick blue trace) and movement (thick red trace) epochs are plotted as a function of depth after realignment based on the CSD of the motor epoch. Thin blue and red traces represent the normalized LFP activity of each individual session. ***D***, The session-averaged visuomotor difference (VMD) is plotted against depth (thick green trace). Thin green traces represent the VMD for individual datasets. ***E***, The session-averaged VMI (purple, same trace as in ***B***) and the VMD (green, same trace as in ***D***) are overlaid. Depth 0 corresponds to the reference channel used to align data across sessions (see Materials and Methods). Shaded regions represent 1 SE around the mean. Negative and positive VMI (and VMD) values denote greater visual- and movement-related activities, respectively.

both signals varied along the dorsoventral axis of the SC in 32 sessions across 3 monkeys (5, 17, and 10 datasets recorded on Monkeys BB, BL, and SU, respectively). We focused on the strengths and onset times of these transient responses during the visual and movement periods. We performed analyses on both individual trials and across-trials average waveforms to determine whether the LFP modulation leads or lags the onset of burst of spikes in the two epochs. Our results highlight the potential importance of performing trial-by-trial analyses, although such signals are hampered by noise.

Laminar organization of spiking activity and local field potentials

Figure 1*A* and Figure 1*B*, respectively, show spike density traces of 10 example trials and the average spike density waveform across all trials for each channel along the SC dorsoventral axis of an individual session. For each plot, the data are aligned on visual burst onsets (left column; for rationale, see Materials and Methods) and saccade onsets (right column) and averaged only across trials when the stimulus was presented in the response field. First, we replicate the depth-dependent effects and main results of our previous work (Massot et al., 2019) but with changes in the CSD-based depth alignment method and trial-by-trial temporal alignment (see Materials and Methods). The burst observed after target presentation was strongest in the superficial layers and decreased gradually for deeper layers. Many neurons, particularly those shown in greenish colors (between channels 9 and 13), also presented sustained activity following the initial burst. The right panel illustrates that SC neurons also produced a robust burst around the time of saccade onset. The amplitude was most vigorous in the intermediate layers and decreased in layers above and below it. Neurons with the most intense saccade-related bursts also exhibited large visual bursts (traces in various shades of green). These observations are captured by the blue and red traces in Figure 1*C*, which denote, respectively, the average normalized and baseline-corrected activities as a function of depth during the visual and movement epochs (Fig. 1*B*, gray shaded regions). Figure 1*D* contrasts the visual and motor activities in terms of the VMI, which revealed the gradual shift from visual dominance in the superficial layers to motor dominance in the intermediate layers. The VMI then plateaued in favor of a motor response for deeper channels.

In addition to the spiking activity, we also analyzed the LFP signals recorded during the same session. Figure 1*E*, *F* shows individual and trial-averaged LFP modulations, following the same configurations used for spike density waveforms. The superficial channels displayed a pronounced stimulus-evoked downward deflection that was gradually attenuated in deeper channels. The saccade-aligned LFP traces followed a similar pattern, but the depth exhibiting the strongest trough within the shaded region occurred a channel or two deeper, and typically after saccade onset. In addition, the LFP waveforms often became positive in deepest channels. This trend was captured on plotting normalized average LFP activities as a function of depth in small windows around visual burst and saccade onsets (Fig. 1*G*). To contrast LFP activities in the two epochs (Fig. 1*H*), we created a new metric denoted VMD (see Materials and Methods). VMD alleviates the requirement for positive signal assumption, as it is the case for VMI, and allows the analysis of LFP signals that may have positive or negative values. For this example session, the trial-averaged LFP in the two epochs followed similar patterns (Fig. 1*G*), with two major differences: (1) for each channel, the trough modulation in the movement epoch was not as strong as in the visual epoch; and (2) across depths, the largest modulation occurred slightly deeper in the movement epoch. These observations are quantitatively captured by the VMD measure, which displays an abrupt transition from visual to motor preference (Fig. 1*H*, channel 9). This transition occurs at several channels deeper than the transition in the VMI computed from spiking activity (Fig. 1*D*, channel 13).

We also explored qualitatively whether spiking and LFP activity share comparable temporal dynamics across the SC layers. Figure 1*I* shows trial-averaged, normalized spiking and LFP activity during the visual (top row) and motor (bottom row) epochs for four different channels (from superficial (leftmost) to deep (rightmost) channels). The LFP activity is inverted (multiplied by −1) for better visualization. We observed that LFP activity and spiking signal share the same trend on both visual and motor epochs in a superficial channel (first column). A common pattern is found on the visual epoch but not during the motor epoch in an intermediate channel (third and four column). Indeed, we observed that, in the motor epoch, the beginning of the LFP modulation is delayed compared with the spiking activity and the maximum modulation appeared later. In deeper channels (two right columns), the two signals seem to follow different trends in both epochs. Together, these observations exclude the idea that LFP activity is merely a reflection of the spiking activity.

We observed similar trends in most datasets and sought a way to average them across sessions. We used CSD analyses to identify a marker of SC depth that could be used to align the data across multiple sessions (for more details, see Materials and Methods). Figure 2*F* shows a CSD plot obtained from the LFP signals aligned on saccade onset (Fig. 2*G*) for one session. Negative and positive values correspond to current sinks and sources, respectively. Snippets (200 ms window around saccade onset represented by Fig. 2*F*, purple dashed square) of CSD plot from five different datasets are shown in Figure 2*H*. In every session, we can identify a reversal between sink (in red) and source (in blue) currents around the time of saccade onset. The channel at which this transition occurred was defined as the reference channel and used to align the different datasets. Figure 2*I* (left) shows these five datasets aligned relative to their reference channels. Figure 2*H* is a snippet of Figure 2*F*. Figure 2*I* shows the VMD for these five different datasets before (Fig. 2*I*, left) and after realignment (Fig. 2*I*, right). The dispersion in VMD traces is visibly reduced after the realignment.

We also realigned the dataset based on CSD plot obtained from LFP aligned on target onset. During the visual epoch, the switch between sink and source was not consistent across datasets. Thus, we used the "hotspot" (strongest sink activity) as a marker to align data across sessions (Fig. 2, left panels). Figure 2*A* shows a CSD plot obtained from the LFP signals aligned on target onset (Fig. 2*B*) for one session. Snippets (200 ms window after target onset) of CSD plots from five different datasets are shown before and after alignment on the hotspot (Fig. 2*C*,*D*), and the impact of this procedure on the VMD is illustrated in Figure 2*E*. After realignment the crossing points were scattered less across depth. We decided to use CSD on motor epoch rather than on visual epoch to realign data because the pattern of activity was more consistent across datasets. Realigning the data using the visual epoch does not change the results. For CSD on the visual epoch, the data were not aligned on the visual burst but on the target onset. The purpose of aligning the data on visual burst was to reduce the time variability between trials. The CSD analysis, to a large extent, is not sensitive to the trial-to-trial relative timings. Indeed, the CSD algorithm is a spatial analysis more than a temporal analysis. Moreover, by using the target onset (which is an external event as the saccade onset) to align the individual trials, we were able to average across all trials and generate a smoother representation of the raw LFP activity.

To better visualize how activity features change continuously with depth, rather than across discrete contacts, we applied linear interpolation to the signals between channels. The resulting depth values are then reported in μm, not channels or contacts. Results are presented between −1200 and 1200 μm with respect to the "reference channel," spanning ∼17 channels. The outcomes of the CSD-guided alignment (based on the reversal in the motor epoch) and interpolation on firing rates and LFP activity in the visual and movement epochs are shown in Figure 3. The visual spiking activity peaked 447 μm above the reference channel (mean amplitude ± SEM: 0.220 ± 0.024 normalized spk/s) and then gradually decreased for more dorsal and ventral depths (Fig. 3*A*, blue trace). The movement spiking activity remained relatively high from ∼280 μm above to 310 μm below the reference depth, with a peak at −302 μm (mean amplitude ± SEM: 0.525 ± 0.050 normalized spk/s), and gradually decreased for more dorsal and ventral locations (Fig. 3*A*, red trace). Potent LFP modulation during the visual epoch was observed at ∼360-900 μm above the reference channel, with strongest trough observed at 749 μm (mean amplitude ± SEM: −0.290 ± 0.044 normalized μV). The LFP modulation approached baseline values for more ventral locations (Fig. 3*C*, blue trace). During the movement epoch, LFP trough was greatest at 449 μm above the reference depth (mean amplitude ± SEM: −0.201 ± 0.033 normalized μV). The signal returns to baseline and even turns positive ventrally (Fig. 3*C*, red trace). For deeper locations, the movement LFP activity peaks at −452 μm (mean amplitude ± SEM: −0.162 ± 0.021 normalized μV). It is important to note that for deeper depths the visual average activity is close to zero, whereas the motor average activity is consistently positive. The magnitude of the motor trough at superficial locations is higher than the magnitude of the motor peak at deeper locations. Overall, these results show that the amplitudes of modulation (i.e., "peak" and "trough") are systematically organized across depths. The visual peak spiking activity (447 μm) is situated at 749 μm more dorsally than the region of strong motor spiking

activity (–302 μm), reflecting a visual preference for superficial layers and movement preference for deeper layers. For the LFP signal, the maximum trough modulation during the visual epoch is situated 300 μm more dorsally than the trough LFP activity during movement epoch (between depths 749 and 449 μm). In deeper layers, the peak LFP activity (positive modulation) during the movement epoch is situated at –452 μm relative to the reference depth, whereas the visual LFP activity plateaus close to zero value. These features reflect a visual preference for dorsal locations and movement preference for ventral locations, for both spikes and LFPs.

We further quantified this dorsoventral organization through the VMI and VMD on spiking and LFP activities, respectively (see Materials and Methods). The analysis confirms across all sessions the trends observed in the individual session distributions (Fig. 3*B*,*D*). The VMI transitioned linearly from visual preference at dorsal sites to motor dominance at intermediate depths but then plateaued for deeper sites. The VMD was negative at most dorsal sites, exhibited a slight trend toward less negative values at the reference depth, and then switched toward positive values and decreased modestly for deeper layers.

Next, we sought to quantify the depth at which the VMI and VMD switched from visual-dominant to movement-dominant responses. The mean and SE of the VMI (Fig. 3*B*) and VMD (Fig. 3*D*) patterns, shown as thick traces and shaded regions, respectively, reveal a gradual shift that matched the individual sessions shown in Figure 1*D*, *H*. Yet, a closer examination of the individual sessions exhibits several crossing points (Fig. 3*B*,*D*, light traces), especially for the VMI. Therefore, we used the bootstrap method to statistically test the average VMI and VMD crossing points. We obtained VMI and VMD profiles for 1000 iterations performed with 100% of the data selected randomly with replacement. The bootstrap procedure revealed that the switch from visual to movement-related responses occurs deeper for the LFP activity (average depth ± SD: 161 ± 137 μm) compared with the spiking activity (average depth ± SD: 665 ± 102 μm). This difference is statistically significant (two-sample *t* test, $p < 0.01$).

We also computed the d' metric (see Materials and Methods) to quantify the visuo-motor dominance of spiking activity (data not shown). We observed a similar trend as that observed for the VMI. Applying the same analysis to the LFP data were deemed uninterpretable because the LFP can assume positive or negative values. We also repeated the VMI and VMD analyses on data aligned based on CSD applied on LFP activity during the visual epoch. Overall, the results are similar.

Finally, the average traces in Figure 3 are jagged. Recall that we aligned datasets with different spacings between channels (150 or 200 μm) and applied a linear interpolation between contacts. The result is that, at each depth, the average is computed on different number of values, making the traces less smooth. Corroborating this explanation, the traces in Figures 5-8 are more jagged compared with the ones in Figure 3 because of higher variability in the number of recorded values at each depth.

Modulation onset times in spikes and LFP signals

The VMI and VMD analyses were performed on average spike density and LFP patterns of each session. If we had performed the computation on individual trials and then averaged across trials, we would have obtained identical results because these are linear operations. For the next set of analyses, we sought to detect burst onset in the spiking activity and modulation onset in the LFP to determine whether the spikes lead or lag the LFP. Here, the average onset times on each trial need not equal the onset time of the average trial. Hence, we performed analyses on both individual trials and across-trials average; and indeed, we found small but functionally important differences.

Figure 4 illustrates our method for determining modulation onset. The same procedure was used on individual trials (2 examples shown in Fig. 4*A*,*B*) and across trials average (Fig. 4*C*, *D*) of both the spiking (Fig. 4*A*,*C*) and LFP activities (Fig. 4*B*,*D*). A continuous, piecewise linear regression was applied on a snippet of activity that ended at or near the time of the peak of the spiking activity or the trough of the LFP signal (gray shaded areas; for details see Materials and Methods). The inflection point was used as the onset of the modulation. In Figure 4*C*, *D*, the red crosses correspond to the inflection points detected on the average activity, while the blue crosses correspond to the average of the inflection points detected on individual trials (blue circles). For this particular example, the onset of LFP activity was detected slightly earlier in the trial-by-trial analysis than during the average analysis (Fig. 4*D*, blue cross ahead of red cross). In contrast, the onsets were nearly identical on the spiking signal (Fig. 4*C*, red cross and blue cross overlap).

Figure 5*A* shows how the onset times of spike bursts (red) and LFP modulations (blue) during the visual epoch detected on individual trials varied with depth, relative to each session's reference channel identified with our CSD-based realignment procedure. Also shown in the same format is the variance accounted for (R^2 metric; Fig. 5*B*) by the piecewise linear fit; it is higher in the top half of the SC. For each trial, the onset of the spike burst on the reference channel was defined to occur at time 0. Onset times on all other channels as well as the LFP data were referenced to this spike-based measurement of time and depth. Each thin trace represents the average of the onset times measured on individual trials from one session, while the thick traces and accompanying shaded regions denote the across-sessions average and 1 SEM. The data indicate that, during the visual epoch, the onset of the spiking activity occurs after the onset of the LFP activity in the dorsal half of the SC (positive depth values). To quantify this observation, we computed the relative timing for each session, defined as the LFP modulation onset time minus the spike burst onset time. A negative value indicates that the LFP modulation occurs earlier than the spike burst (i.e., LFP leads), and a positive value suggests that the LFP modulation occurs after the spike burst (i.e., spike leads). Figure 5*E* shows that the relative timing is negative and statistically different from zero for the superficial layers (from 1200 to –331 μm) with an average relative timing of –8 ms (one-sample *t* test without correction, $p < 0.05$, indicated as black shaded portion of the middle line on the right). As the LFP signals are not independent across depth, we also applied a correction method to counteract the multiple comparisons problem and control the family-wise error rate. We tested two different correction methods: one-sample *t* test with Bonferroni correction at every 150 μm (corresponding approximately to the spacing between two contacts) and one-sample *t* test at each depth using the Benjamini–Hochberg procedure (i.e., false discovery rate method). Statistical significance information plotted on the left (gray/black dotted line) reflects the Bonferroni correction, whereas that on the right denotes the Benjamini–Hochberg correction. A statistical difference was found for both correction methods around the same depth (~300 μm). This result shows that LFP modulation leads spike bursts in the dorsal layers during the visual epoch.

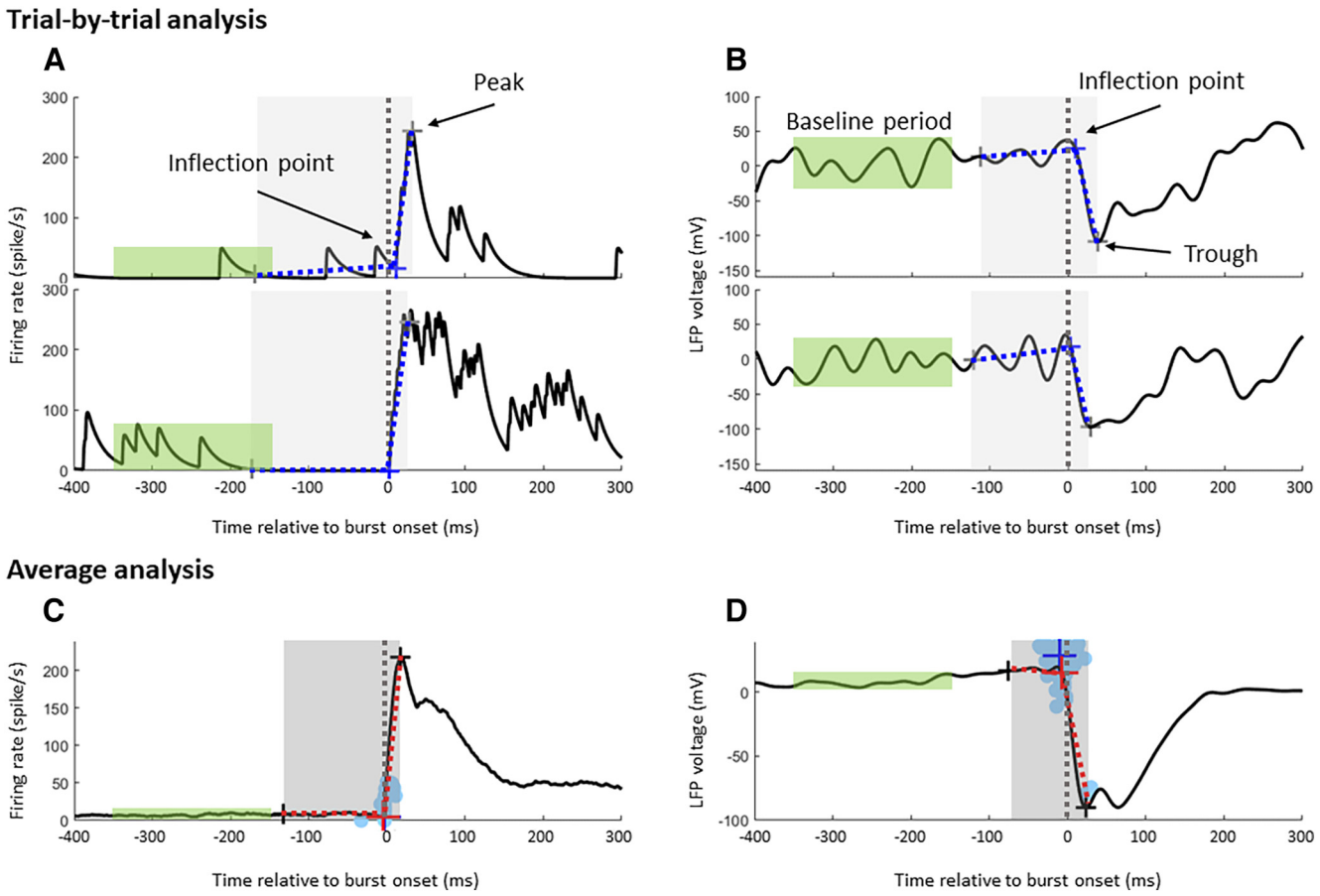

Figure 4. Illustration of piecewise linear regression analysis. ***A***, Spike density traces for two example trials. ***B***, LFP traces recorded on the same contact for the same two trials shown in ***A***. Blue dashed lines indicate the two linear segments produced by the piecewise linear regression. Blue cross represents their intersection (what we call the inflection point and identify as the beginning of the signal modulation). ***C***, Average spike density waveform computed across trials on one probe contact. ***D***, Average LFP traces computed across the same trials on the same channel. Blue dots represent the inflection points of all individual trials. Blue cross represents the average of the individual inflection points. Red dashed lines indicate the two linear segments obtained from the piecewise linear regression applied to the average spike density profile (in ***C***) and the LFP waveform (in ***D***). Red cross represents the inflection point computed on average traces. Red and blue crosses represent superimposed nearly perfectly in ***C*** but not in ***D***. Green shaded area represents the baseline period. Gray shaded area represents the range in which the piecewise linear regression was performed (starting and ending by the black crosses; for details, see Materials and Methods). All traces are aligned on visual burst onset (dotted, vertical gray line in each panel), and recording is shown from the same session and channel.

Next, we repeated the modulation onset analysis on signals averaged across trials (Fig. 5*C–F*), again using the continuous piecewise linear regression method. For each individual channel, we averaged only the trials used in the trial-by-trial analysis. The thin traces plot the onset times as a function of depth for individual sessions, and the thick traces and accompanying shaded regions denote the across-sessions average and 1 SEM (Fig. 5*C*). Unlike the individual trials analysis, the onset of the spiking activity occurs at relatively the same time as the onset of the LFP activity (the red and blue traces overlapped) during the visual epoch, which is supported by viewing the relative timing between the onset times (Fig. 5*F*). When performing a one-sample *t* test ($p < 0.05$, without correction) at each depth, the relative timing was statistically different from zero from 815 to 696 µm and from 498 to 449 µm with very short average relative timing values of 4 and 4 ms, respectively (black portion of the middle line). However, we see that, after multiple comparisons corrections, we do not find consistent statistically significant differences (Fig. 5*F*, gray left and right lines). As before, we computed the R^2 to quantify the goodness of the piecewise linear fits. As observed for individual trials, Figure 5*D* shows that the R^2 metric is higher on superficial depths for both the spiking and the LFP signals. Overall, the results show that the LFP and spike modulation times during the visual epoch are indistinguishable when evaluating signals averaged across trials, but that the LFP modulation consistently leads spike bursts based on an analysis of individual trials. Figure 5*G*, which overlays the average traces from Figure 5*E*, *F*, highlights this distinction. Repeating the analysis with data sessions aligned using the CSD of the visual epoch yielded similar observations (not shown).

We also applied the continuous piecewise linear regression method to detect spike burst onset and LFP modulation during the motor epoch on both individual trials and across-trials average signals. Figure 6 plots these data in the same format as Figure 5. Spiking burst onset preceded saccade onset and the lead time remained relatively constant across depth, in agreement with previous findings (Massot et al., 2019). LFP modulation onset preceded saccade onset in the superficial layers but then reached baseline value (Fig. 6*A*) or even lagged the eye movement in the intermediate and deep layers (Fig. 6*C*). Unlike the visual epoch data, LFP modulation onset did not lead the spike burst (when one was detected) in the superficial layers. In the intermediate and deeper layers, where a burst is the expected signature, the LFP modulation always lagged the spiking burst. Similar effects were observed on individual trials and across-trials average. The relative timing values, based on analyses on individual trials (Fig.

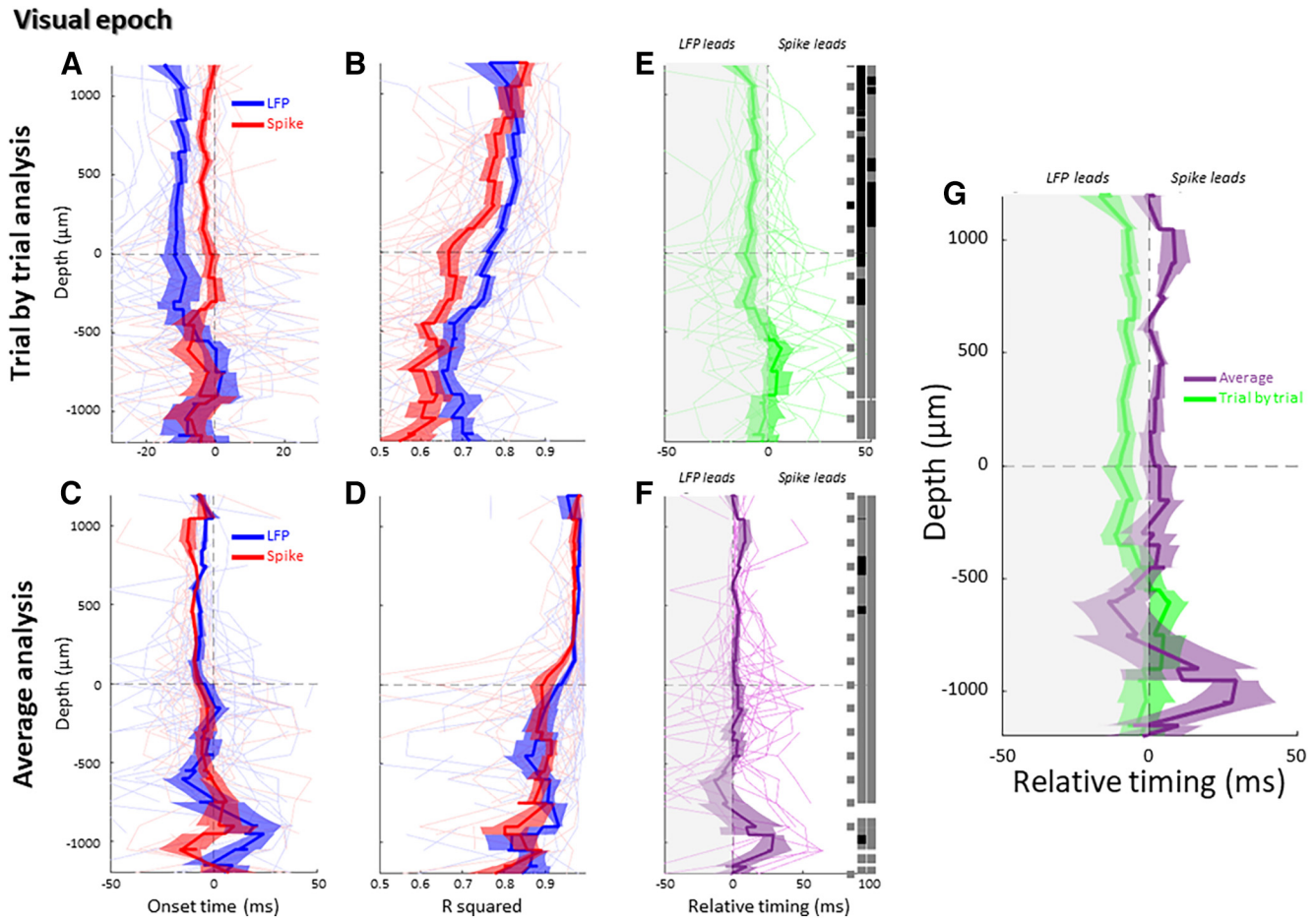

Figure 5. Depth-dependent distribution of onset times in visual spike burst and LFP modulation. Data aligned on CSD of motor epoch. ***A***, The piecewise linear regression was applied to each waveform for each trial and channel. For the subset of trials for which onset times were detected for both signals, we computed the average onset times across trials for each channel. Data from individual sessions are plotted as thin traces (red represents spike burst onset; blue represents LFP modulation onset). Thick traces and shaded regions represent the across sessions mean and 1 SE. ***B***, The goodness of the piecewise linear fit performed on individual trials (R^2) is shown as a function of depth, using the same convention used in ***A***. ***E***, Relative timing between spike burst and LFP modulation onsets times was computed as the difference between each session's blue and red traces from ***A***. Individual session data are plotted as thin traces. The across session mean and 1 SEM are shown as thick trace and the shaded region, respectively. Negative (positive) relative time values indicate that LFP modulation precedes (lags) spike burst onset. The statistical significance of the relative timing with respect to 0 ms was tested in three ways. The middle, vertical line indicates whether the mean relative timing at each depth was significantly different from zero (one-sample *t* test without correction). The spaced squares on its left represent the outcome of the one-sample *t* test with Bonferroni correction applied at each contact (150 μm apart). Right line indicates the result of the one-sample *t* test corrected with the Benjamini–Hochberg procedure. For all statistical tests: Black represents when the test was statistically significant ($p < 0.05$); gray represents not statistically significant. ***C***, For each session, the traces used in the trial-by-trial analysis above were averaged to compute the mean spike density and LFP trace for each channel. The times of burst onset and LFP modulation onset were determined from these traces and plotted as a function of depth (thin traces for each session). Thick traces and shaded regions represent the across sessions average and 1 SE for spikes (red) and LFP (blue) signals. ***D***, The goodness of the piecewise linear fit performed on average traces (R^2) is plotted against depth, using the same convention used in ***C***. ***F***, Relative timing between spike burst and LFP modulation onsets times was computed as the difference between each session's blue and red traces from ***C***. The remaining format is identical to ***E***. ***G***, Thick traces from the relative timing plots (***E***,***F***) computed from the trial-by-trial analysis (***E***) and the average analysis (***F***) are overlaid to facilitate visualization.

6*E*), were statistically different from zero from 532 to −1099 μm with an average relative timing of 25 ms (same results using one-sample *t* test without correction, with Bonferroni correction and Benjamini–Hochberg procedure). For analyses performed on signals averaged across trials (Fig. 6*F*), the relative timing was statistically different from zero from 238 to −1200 μm with an average relative timing of 51 ms (same results using one-sample *t* test without correction, with Bonferroni correction and Benjamini–Hochberg procedure). Figure 6*G* overlays these results. The high R^2 metric in the intermediate and deep layers (Fig. 6*B*,*D*) further indicates that the onset of spiking and LFP modulations occurs simultaneously on both trial-by-trial analysis and average analyses on the superficial layers. In the deeper layers, the spiking activity leads for both analyses, and the lead is even larger on the average analysis (51 ms) than on the trial-by-trial analysis (25 ms). Repeating the analysis with data sessions aligned using the CSD of the visual epoch yielded similar observations (not shown).

Our relative timing analysis thus far was limited to trials and channels for which modulation was detected on both spike and LFP signals. When analyzing waveforms averaged across trials, we could include all trials, not just this subset. Figure 7 superpositions the relative timing distribution computed from an average of all trials (orange trace) with those determined from individual trials (green) and average computed from this subset of trials (purple). In the visual epoch, the relative timing patterns of the two average conditions are very similar in the dorsal half of SC. In the deeper layers, a visual response was often observed in the spiking activity of visuomotor neurons but was often not accompanied by a modulation in the LFPs (see example traces in Fig. 1). This could produce the impression that spikes lead LFPs in these layers of SC. In the motor epoch, in contrast, there is

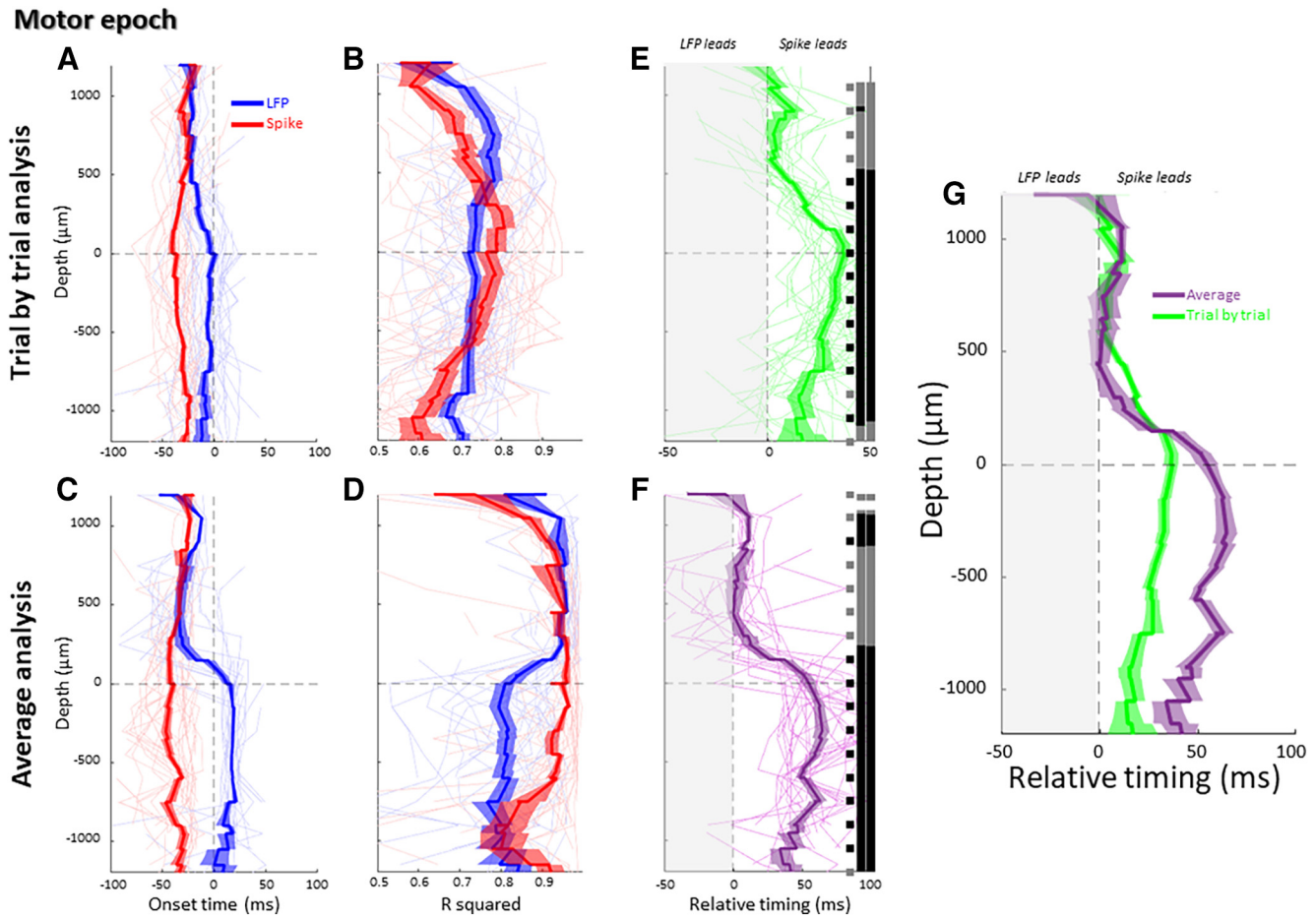

Figure 6. Depth-dependent distribution of onset times in motor spike burst and LFP modulation. Data aligned on CSD of motor epoch. Same display format as in Figure 5, except that the analysis is applied to the movement-related burst in the spike density waveforms and the accompanying modulations in the LFP signal.

effectively no distinction between the two average conditions. We then performed cross-validation by repeating the same analyses separately on even and odd trials (not shown). Overall, the analyses performed on these two groups showed the same pattern.

We also considered whether and how the cutoff frequency of the filter applied to the LFP signal could alter detection of modulation onset, which in turn would impact relative timing. We know from above that for analysis performed on trial-averaged waveforms, the relative onset times are not statistically different from zero in superficial layers for either epoch (Figs. 5*F*,6*F*) when the LFP activity was filtered between 0.7 and 30 Hz. We repeated this analysis on the trial-by-trial traces (Fig. 8*A*,*B*) and trial-averaged profiles (Fig. 8*C*,*D*) for several lowpass cutoff frequencies: 10, 30 (used in preceding analysis) and 100 Hz. We did not find any differences for the cutoff frequency higher than 30 Hz for both the trial-by-trial analysis (Fig. 8*A*,*B*, black and green traces) and the average analysis (Fig. 8*C*,*D*, black and green traces). When the LFP was filtered at 10 Hz, the relative timing was more negative in superficial layers during both the visual and motor epoch than for other filtering frequencies for both the trial-by-trial analysis (Fig. 8*A*,*B*, yellow traces) and the average analysis (Fig. 8*C*,*D*, yellow traces). It means that, with this filtering, the LFP signal is smoother and the LFP onsets were detected earlier. The fact that we do not find any difference between 30 and 100 Hz indicates that 30 Hz cutoff is sufficient and does not compromise the detection of LFP modulation.

Distribution of modulations across depth

We next examined whether the likelihood of detecting modulations on spike and LFP signals varied as a function of depth. We grouped each trial per channel into one of four categories: onsets detected in both spike and LFP signals, onset detected in the spike trace but not in the LFP, modulation onset detected in the LFP signal but not in the spike signal, and no modulation onsets detected in either of the two signals. Figure 9*A*,*B* shows the percentages of these four groups across all the datasets and across all channels combined. We detected both spike and LFP onset times in 18% and 22% of cases during the visual and the motor epochs, respectively. It was less common to detect LFP modulation without a spike burst (9% and 4% for visual and motor epoch, respectively). Cases where we detected neither spike bursts nor LFP modulations were most frequent (40% and 39% for visual and motor epoch, respectively). The percentage of signals with spike bursts without LFP modulation was lower (32% and 39% for visual and motor epoch, respectively). Figure 9*C*,*D* shows the four categories as a function of depth after CSD-based realignment. As shown in Figure 9*A*,*B*, the case where we detected LFP onset without burst onset corresponds to the lowest percentage during both the visual and motor epochs. These detections are uniformly distributed across depth (Fig. 9*C*,*D*, blue traces), suggestive of false detections. Cases in which detection was absent on both signals tended to occur at the two ends of the dorsoventral axis, potentially indicative of track locations outside of the SC and/or loci where the magnitude of modulation was weak (green

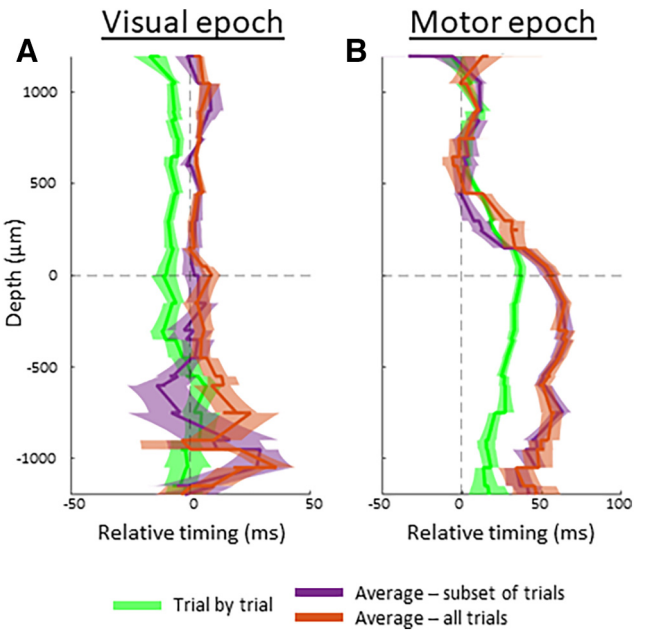

Figure 7. Relative timing performed on different subsets of trials. Relative timing plots during the visual (***A***) and motor (***B***) epochs from the average analysis. Green and purple traces represent the trial-by-trial analysis and the average analysis (as shown in Figures 5 and 6), respectively. Purple trace represents the average activity based only on trials and channels used for the trial-by-trial analysis. Red trace represents the relative timing computed on average activity computed across all trials.

traces). The distribution of signals in Figure 1 suggests that LFP modulation is strongest in the superficial layers during the visual epoch. Of course, visual bursts on the spiking channel are also ubiquitous. This combination can be appreciated in Figure 9*C* as a high percentage of spike burst and LFP modulation signals in the superficial layers (black traces). The red traces, which denote burst detection in spiking activity but not in the LFP, peak in the deeper layers, which align with the LFP signal returning close to baseline values at these depths. In contrast, visuomotor neurons in these layers exhibit strong bursts in both epochs.

Discussion

We analyzed the spatial distributions and temporal properties of spiking and LFP activities recorded simultaneously in the macaque SC. We showed with a laminar electrode that the LFP signal reveals a visual preference for superficial layers and a movement preference for deeper layers (Figs. 1 and 3), comparable to features of the spiking activity. Although these two signals share a common general visuomotor pattern along the dorsoventral axis of the SC, the switch from the visual to the motor preference happens deeper on the LFP signal (Fig. 3*E*). Moreover, the analysis of the timing of their phasic responses on individual trials showed that the onset of LFP modulation occurs slightly earlier than the sensory burst in visually responsive layers (Fig. 5*E*, green trace). In contrast, the motor burst strongly leads LFP onset in deeper layers for both trial-by-trial and across-trials average analyses (Fig. 6*E*, green and purple traces).

Sensorimotor features along the dorsoventral axis of SC

It is well known that the spiking activity in the SC shows a characteristic sensorimotor transformation along its dorsoventral axis. Indeed, single-contact as well as multicontact electrode studies have shown that the neurons located in the superficial

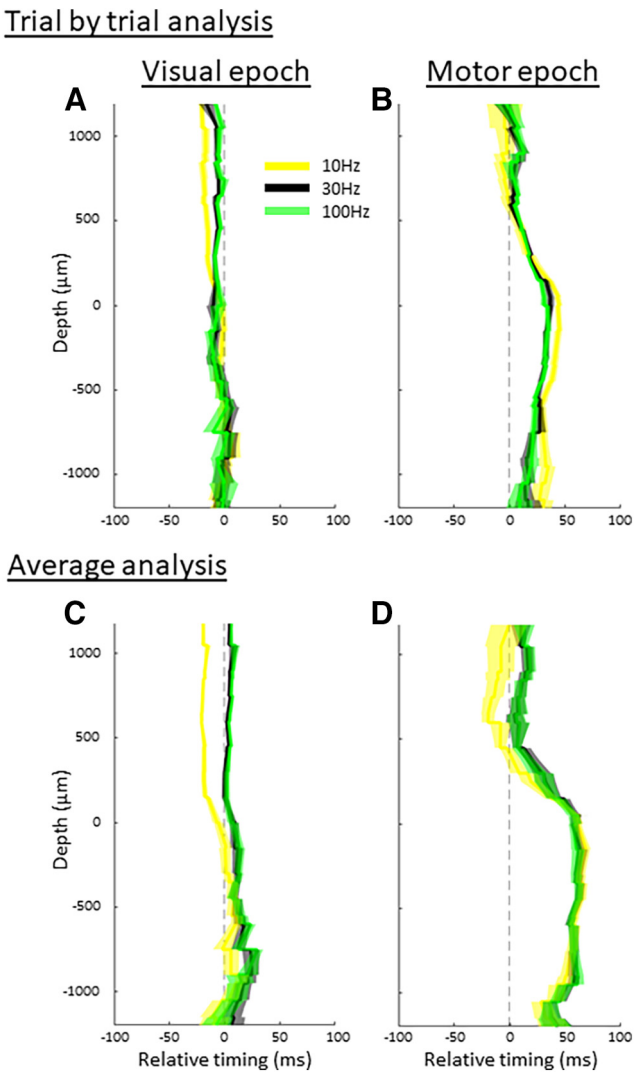

Figure 8. Relative timing distributions for different lowpass cutoff frequencies. Relative timing as a function of depth performs during the visual (***A***,***C***) and motor (***B***,***D***) epochs from the trial-by-trial (***A***,***B***) and the average analysis (***C***,***D***). The LFP activity used for all the previous figures was bandpass filtered between 0.7 and 30 Hz (black traces). We also used other cutoff frequencies (10 and 100 Hz) represented by different colors (yellow and green, respectively).

layers display sensory-related activity, while those in the deeper layers exhibit a more motoric response (Mohler and Wurtz, 1976; Mays and Sparks, 1980; Massot et al., 2019). Using single-unit recordings, Ikeda et al. (2015) reported that the LFP activity follows a similar pattern along the dorsoventral axis of SC. In our study, which used a multicontact laminar probe, we also observed largely similar visuomotor patterns across depth found in both LFP and spike density waveforms, except for one key distinction: the switch from the visual to the motor preference happens deeper on the LFP activity compared with the spiking signal. This spatial shift was not found in the previous study (Ikeda et al., 2015) probably because the sampling bias of single-electrode studies is typically focused on intermediate layer neurons.

Interestingly, the loci at which the VMI and VMD cross over from visual to motor dominance are linked to specific features in the LFP and spike signals, respectively (Fig. 3). The depth at which spiking activities in the visual and motor epochs are comparable (VMI = 0) is also the region where visual LFP

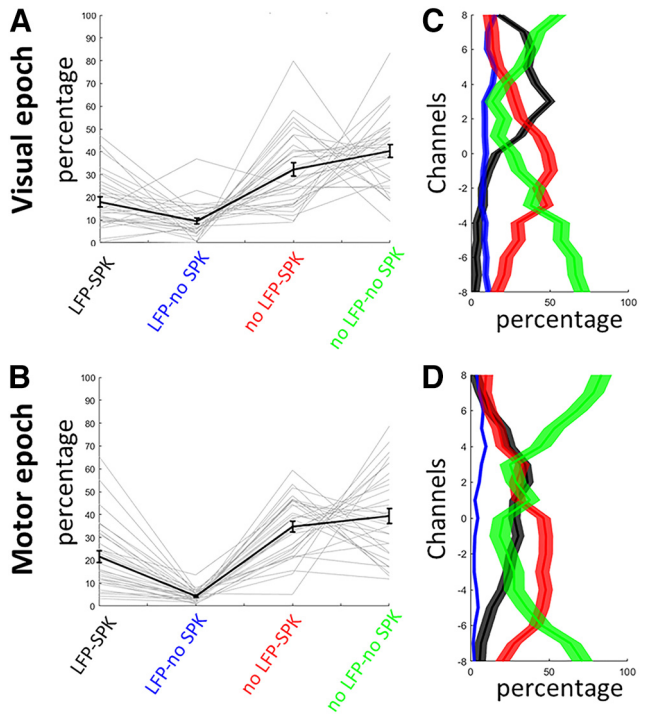

Figure 9. Distribution of spike and LFP onset detections. Each trial per channel was grouped into one of four categories: onsets detected in both spike and LFP (LFP-SPK); onset detected in the LFP but not in the spike (LFP-no SPK); onset detected in the spike but not in the LFP (no LFP-SPK); and no modulation onsets detected in either of the two signals (no LFP-no SPK). ***A***, ***B***, Percentages of these four groups across all the datasets and across all channels combined (black thick line) during the visual and the motor epoch, respectively. Thin lines indicate the percentages of the individual datasets. ***C***, ***D***, Percentages of trials in the four categories at each depth after CSD-based realignment using the motor epoch. The different colors represent the different categories.

modulation is most robust. This is likely the region spanning the ventral superficial layers, the optic layer, and the dorsal intermediate layers. Conversely, the crossover in the LFP-based VMD metric occurs at depths where the saccade-related burst is most vigorous. This is likely at the interface of the intermediate and deeper layers. Thus, the zero crossings of VMI and VMD appear to be a proxy of layers producing the strongest visual LFP modulation and motor spike bursts, respectively.

Relative timing of spiking activity and LFP

Whereas spikes represent the output activity of the recorded neurons, the nature of the LFP signal is unclear. By definition, LFP is the aggregate voltage activity produced by all elements surrounding the recording site. One particular hypothesis states that it represents predominantly the focal synaptic activity of the inputs at the recording site (Mitzdorf, 1985; Buzsáki, 2004; Logothetis and Wandell, 2004; Buzsáki et al., 2012). In this framework, one might expect the LFP modulation to precede the spiking activity, especially for the visual epoch. This question has been addressed previously in the FEFs in the context of memory-guided saccades (Sendhilnathan et al., 2017) and visual search task (Monosov et al., 2008). Both studies reported that the LFP signal leads spiking activity during the visual response, while the reverse order is observed during the motor epoch. For the memory-guided saccade study, which is more comparable to our implementation, LFP modulation precedes the visual spike burst on average by ~20 ms and the motor spike burst leads LFP by ~130 ms. A previous SC study reported that the onset times of spike burst and LFP modulation during the visual epoch were not statistically different from each other (Ikeda et al., 2015); a comparable analysis on the motor epoch was not provided. These previous analyses in both SC and FEF were performed on signals averaged across trials. In our study, the visual LFP modulation in superficial and intermediate layers leads the visual spike burst by only ~8 ms and only when the analysis was performed on individual trials; the relative timing was not significantly different from zero when we analyzed signals averaged across trials, in agreement with Ikeda et al. (2015). During the motor epoch, the spike burst leads LFP modulation by ~25 ms (individual trial analysis) or ~50 ms (across trials average). Additionally, these previous studies used a threshold method to detect modulation onset. We attempted this method in our initial pilot analyses and observed many cases in which the onset times were overestimated or underestimated because of the noisy nature of biological signals. We therefore decided to use the piecewise method for its more conservative aspect. Collectively, these results highlight the sensitivity and caveats of timing detection analyses, for both individual trials and across-trials averages.

Overall, we view the SC and FEF results to be comparable in terms of relative timing of LFP and spike modulations in both visual and movement epochs, although the lag/lead times are smaller in the SC. The results argue in favor of an efficient and almost instantaneous input-output transformation between LFP modulation and spike burst in the superficial layers activity during sensation. Indeed, if the LFP modulation triggers the spike burst, the signal transduction could be rapid and show a very short processing time between LFP modulation and spike burst onsets. Such processing may facilitate the fast and efficient visuomotor transformation required for the generation of express saccades (Aizawa et al., 1999; Kurata and Aizawa, 2004) or for the adjustment of additional movements in foraging or sequential saccade tasks (Basu et al., 2021; Mirpour and Bisley, 2021; Sendhilnathan et al., 2021).

Given the small lead time of LFP modulation over spike burst in the visual epoch and only for the individual trials analysis, the skeptical reader may justifiably entertain the alternate hypothesis that the LFP simply reflects, and thus is simultaneous with, the spiking activity at the recording site. Our counterargument is that, if the LFP were solely a reflection of the output of the neurons, then we should observe similar patterns on both signals in both visual and motor epochs. Indeed, Ikeda et al. (2015) have shown such examples. In accordance, we show that, on relatively superficial channels, the spike and the LFP traces modulate in phase during both the visual and the motor periods (Fig. 1*I*, left). In contrast, the spiking and LFP signals are not a mirror copy of each other for deeper channels (Fig. 1*I*, right panels). This finding supports the idea that the LFPs do not merely reflect the spike rate produced by nearby neurons.

Modulation onset detection performed on individual trials and across trials average did not produce the same result. Indeed, the average of all onset times detected on individual trials need not equal the onset of the modulation on the trace computed by averaging the individual waveforms. This is because the average trace becomes a smooth version of the individual traces that are not aligned on modulation onset. These differences indicate that detecting a peak in an average profile leads to a misrepresentation of trial-by-trial peak detections (Stokes and Spaak, 2016; Dames et al., 2017; Banerjee et al., 2018). Thus, effort should be made to analyze individual trials (Banerjee et al., 2010)

when the potential of such confounds exists and, especially, when the magnitude of effect is small. In our data, the difference in detection times swayed in favor for earlier LFP modulation for trial-by-trial analysis.

A reliable method of detecting temporal events in LFP and spike trains on individual trials has the potential to provide deeper insights into input-output relationships at the recorded site. Although we studied this effect on bursting activity during the visual and motor epochs, it can in theory be extended also to more modest modulations associated with cognitive processes. In spatial attention tasks, for example, previous work in FEF reported no statistical difference in the temporal order between spikes and LFP for selecting the target during visual search (Cohen et al., 2009; Heitz et al., 2010; Purcell et al., 2013). Importantly, the analysis relied on waveforms averaged across trials and for targets presented in the preferred and antipreferred locations. We speculate that a timing difference could be realized more precisely if the analysis can be performed reliably on individual trials. We note that such experiments are challenging because they require that neural activity be recorded simultaneously from both hemispheres; moreover, the recorded signals have reasonable signal-to-noise ratio to permit such analyses. This analytical framework can also be extended to other cognitive processes, such as performance monitoring; perhaps it will reveal a systematic but different relationship in the temporal features between LFP and spiking activity on individual, correct and error trials (Shen and Paré, 2007; Purcell et al., 2012; Fu et al., 2023). Analyses that consider both types of signals may also reveal neural differences for movements that are goal-directed or not (Sendhilnathan et al., 2021), generated into or out of the neuron's response field (Purcell et al., 2012; Heusser et al., 2022), are context-dependent (Sato et al., 2001; Katnani and Gandhi, 2013; Sadeh et al., 2018), or produced during learning (Bourrelly et al., 2016). In the context of the double step task, a corollary discharge is sent from the SC to the FEF, transiting via the MD (Sommer and Wurtz, 2002). In turn, the FEF will send a signal back to the SC to adjust the upcoming saccade. During or right after the first saccade is made, we would expect to observe LFP modulations (reflecting the corollary discharge) in both the MD and the FEF, whereas, before the second saccade, we hypothesize a lead by the LFP activity over the spikes in the SC. This lead would reflect the signal sent from the FEF to the intermediate layers of the SC. During saccade adaptation, there is little change in the spiking activity of individual SC neurons that burst during saccades (Quessy et al., 2010); rather, temporal control over activation of the rostral SC seems to be the more prominent mechanism (Kaku et al., 2009; Soetedjo et al., 2009; Kojima and Soetedjo, 2018). Perhaps LFPs recorded in the SC may systematically change during saccade adaptation and be more informative than spiking activity. Finally, we also believe that our understanding of online control of saccades may improve by incorporating the LFP. A group of models propose that feedback from the pontomedullary reticular formation controls temporal features of the saccade-related burst of SC neurons (Waitzman et al., 1991; Arai et al., 1994; Keller and Edelman, 1994; Smalianchuk et al., 2018). We speculate that the LFP signal observed during saccades may show signatures of burst suppression, ideally on a trial-by-trial basis. Thus, integrating LFPs with spiking activity on individual trials may improve our understanding of how the SC operates on the sensation-cognition-action axis.

References

Aizawa H, Kobayashi Y, Yamamoto M, Isa T (1999) Injection of nicotine into the superior colliculus facilitates occurrence of express saccades in monkeys. J Neurophysiol 82:1642–1646.

Arai K, Keller EL, Edelman JA (1994) Two-dimensional neural network model of the primate saccadic system. Neural Netw 7:1115–1135.

Banerjee A, Dean HL, Pesaran B (2010) A likelihood method for computing selection times in spiking and local field potential activity. J Neurophysiol 104:3705–3720.

Banerjee A, Kikuchi Y, Mishkin M, Rauschecker JP, Horwitz B (2018) Chronometry on spike-LFP responses reveals the functional neural circuitry of early auditory cortex underlying sound processing and discrimination. eNeuro 5:ENEURO.0420-17.2018.

Basso MA, May PJ (2017) Circuits for action and cognition: a view from the superior colliculus. Annu Rev Vis Sci 3:197–226.

Basu D, Sendhilnathan N, Murthy A (2021) Neural mechanisms underlying the temporal control of sequential saccade planning in the frontal eye field. Proc Natl Acad Sci USA 118:e2108922118.

Bourrelly C, Quinet J, Cavanagh P, Goffart L (2016) Learning the trajectory of a moving visual target and evolution of its tracking in the monkey. J Neurophysiol 116:2739–2751.

Bryant CL, Gandhi NJ (2005) Real-time data acquisition and control system for the measurement of motor and neural data. J Neurosci Methods 142:193–200.

Buzsáki G (2004) Large-scale recording of neuronal ensembles. Nat Neurosci 7:446–451.

Buzsáki G, Anastassiou CA, Koch C (2012) The origin of extracellular fields and currents: EEG, ECoG, LFP and spikes. Nat Rev Neurosci 13:407–420.

Chen CY, Hafed ZM (2018) Orientation and contrast tuning properties and temporal flicker fusion characteristics of primate superior colliculus neurons. Front Neural Circuits 12:58.

Cohen JY, Heitz RP, Schall JD, Woodman GF (2009) On the origin of event-related potentials indexing covert attentional selection during visual search. J Neurophysiol 102:2375–2386.

Cooper B, McPeek RM (2021) Role of the superior colliculus in guiding movements not made by the eyes. Annu Rev Vis Sci 7:279–300.

Dames KD, Smith JD, Heise GD (2017) Averaging trials versus averaging trial peaks: impact on study outcomes. J Appl Biomech 33:233–236.

Drucker CB, Carlson ML, Toda K, DeWind NK, Platt ML (2015) Non-invasive primate head restraint using thermoplastic masks. J Neurosci Methods 253:90–100.

Fu Z, Sajad A, Errington SP, Schall JD, Rutishauser U (2023) Neurophysiological mechanisms of error monitoring in human and non-human primates. Nat Rev Neurosci 24:153–172.

Gandhi NJ, Katnani HA (2011) Motor functions of the superior colliculus. Annu Rev Neurosci 34:205–231.

Godlove DC, Maier A, Woodman GF, Schall JD (2014) Microcircuitry of agranular frontal cortex: testing the generality of the canonical cortical microcircuit. J Neurosci 34:5355–5369.

Hanes DP, Thompson KG, Schall JD (1995) Relationship of presaccadic activity in frontal eye field and supplementary eye field to saccade initiation in macaque: Poisson spike train analysis. Exp Brain Res 103:85–96.

Heitz RP, Cohen JY, Woodman GF, Schall JD (2010) Neural correlates of correct and errant attentional selection revealed through N2pc and frontal eye field activity. J Neurophysiol 104:2433–2441.

Heusser MR, Bourrelly C, Gandhi NJ (2022) Decoding the time course of spatial information from spiking and local field potential activities in the superior colliculus. eNeuro 9:ENEURO.0347-22.2022.

Ikeda T, Boehnke SE, Marino RA, White BJ, Wang CA, Levy R, Munoz DP (2015) Spatio-temporal response properties of local field potentials in the primate superior colliculus. Eur J Neurosci 41:856–865.

Jagadisan UK, Gandhi NJ (2022) Population temporal structure supplements the rate code during sensorimotor transformations. Curr Biol 32:1010–1025.e9.

Kaku Y, Yoshida K, Iwamoto Y (2009) Learning signals from the superior colliculus for adaptation of saccadic eye movements in the monkey. J Neurosci 29:5266–5275.

Katnani HA, Gandhi NJ (2011) Order of operations for decoding superior colliculus activity for saccade generation. J Neurophysiol 106:1250–1259.

Katnani HA, Gandhi NJ (2013) Time course of motor preparation during visual search with flexible stimulus-response association. J Neurosci 33:10057–10065.

Keller EL, Edelman JA (1994) Use of interrupted saccade paradigm to study spatial and temporal dynamics of saccadic burst cells in superior colliculus in monkey. J Neurophysiol 72:2754–2770.
Khademi F, Chen CY, Hafed ZM (2020) Visual feature tuning of superior colliculus neural reafferent responses after fixational microsaccades. J Neurophysiol 123:2136–2153.
Khanna SB, Snyder AC, Smith MA (2019) Distinct sources of variability affect eye movement preparation. J Neurosci 39:4511–4526.
Kojima Y, Soetedjo R (2018) Elimination of the error signal in the superior colliculus impairs saccade motor learning. Proc Natl Acad Sci USA 115: E8987–E8995.
Krauzlis RJ (2005) The control of voluntary eye movements: new perspectives. Neuroscientist 11:124–137.
Kurata K, Aizawa H (2004) Influences of motor instructions on the reaction times of saccadic eye movements. Neurosci Res 48:447–455.
Logothetis NK, Wandell BA (2004) Interpreting the BOLD signal. Annu Rev Physiol 66:735–769.
Maier A, Aura CJ, Leopold DA (2011) Infragranular sources of sustained local field potential responses in macaque primary visual cortex. J Neurosci 31:1971–1980.
Massot C, Jagadisan UK, Gandhi NJ (2019) Sensorimotor transformation elicits systematic patterns of activity along the dorsoventral extent of the superior colliculus in the macaque monkey. Commun Biol 2:287.
Mays LE, Sparks DL (1980) Dissociation of visual and saccade-related responses in superior colliculus neurons. J Neurophysiol 43:207–232.
Mirpour K, Bisley JW (2021) The roles of the lateral intraparietal area and frontal eye field in guiding eye movements in free viewing search behavior. J Neurophysiol 125:2144–2157.
Mitzdorf U (1985) Current source-density method and application in cat cerebral cortex: investigation of evoked potentials and EEG phenomena. Physiol Rev 65:37–100.
Mohler CW, Wurtz RH (1976) Organization of monkey superior colliculus: intermediate layer cells discharging before eye movements. J Neurophysiol 39:722–744.
Monosov IE, Trageser JC, Thompson KG (2008) Measurements of simultaneously recorded spiking activity and local field potentials suggest that spatial selection emerges in the frontal eye field. Neuron 57:614–625.
Nandy AS, Nassi JJ, Reynolds JH (2017) Laminar organization of attentional modulation in macaque visual area V4. Neuron 93:235–246.
Nicholson C, Freeman JA (1975) Theory of current source-density analysis and determination of conductivity tensor for anuran cerebellum. J Neurophysiol 38:356–368.
Pettersen KH, Devor A, Ulbert I, Dale AM, Einevoll GT (2006) Current-source density estimation based on inversion of electrostatic forward solution: effects of finite extent of neuronal activity and conductivity discontinuities. J Neurosci Methods 154:116–133.
Purcell BA, Weigand PK, Schall JD (2012) Supplementary eye field during visual search: salience, cognitive control, and performance monitoring. J Neurosci 32:10273–10285.
Purcell BA, Schall JD, Woodman GF (2013) On the origin of event-related potentials indexing covert attentional selection during visual search: timing of selection by macaque frontal eye field and event-related potentials during pop-out search. J Neurophysiol 109:557–569.
Quessy S, Quinet J, Freedman EG (2010) The locus of motor activity in the superior colliculus of the rhesus monkey is unaltered during saccadic adaptation. J Neurosci 30:14235–14244.
Rasch MJ, Gretton A, Murayama Y, Maass W, Logothetis NK (2008) Inferring spike trains from local field potentials. J Neurophysiol 99:1461–1476.
Sadeh M, Sajad A, Wang H, Yan X, Crawford JD (2018) The influence of a memory delay on spatial coding in the superior colliculus: is visual always visual and motor always motor? Front Neural Circuits 12:74.
Sajad A, Sadeh M, Crawford JD (2020) Spatiotemporal transformations for gaze control. Physiol Rep 8:e14533.
Sato T, Murthy A, Thompson KG, Schall JD (2001) Search efficiency but not response interference affects visual selection in frontal eye field. Neuron 30:583–591.
Sendhilnathan N, Basu D, Murthy A (2017) Simultaneous analysis of the LFP and spiking activity reveals essential components of a visuomotor transformation in the frontal eye field. Proc Natl Acad Sci USA 114:6370–6375.
Sendhilnathan N, Basu D, Goldberg ME, Schall JD, Murthy A (2021) Neural correlates of goal-directed and non-goal-directed movements. Proc Natl Acad Sci USA 118:e2006372118.
Shen K, Paré M (2007) Neuronal activity in superior colliculus signals both stimulus identity and saccade goals during visual conjunction search. J Vis 7:15.1.
Smalianchuk I, Jagadisan UK, Gandhi NJ (2018) Instantaneous midbrain control of saccade velocity. J Neurosci 38:10156–10167.
Soetedjo R, Fuchs AF, Kojima Y (2009) Subthreshold activation of the superior colliculus drives saccade motor learning. J Neurosci 29:15213–15222.
Sommer MA, Wurtz RH (2002) A pathway in primate brain for internal monitoring of movements. Science 296:1480–1482.
Sparks DL (1986) Translation of sensory signals into commands for control of saccadic eye movements: role of primate superior colliculus. Physiol Rev 66:118–171.
Stokes M, Spaak E (2016) The importance of single-trial analyses in cognitive neuroscience. Trends Cogn Sci 20:483–486.
Thompson KG, Hanes DP, Bichot NP, Schall JD (1996) Perceptual and motor processing stages identified in the activity of macaque frontal eye field neurons during visual search. J Neurophysiol 76:4040–4055.
Waitzman DM, Ma TP, Optican LM, Wurtz RH (1991) Superior colliculus neurons mediate the dynamic characteristics of saccades. J Neurophysiol 66:1716–1737.
Waldert S, Lemon RN, Kraskov A (2013) Influence of spiking activity on cortical local field potentials. J Physiol 591:5291–5303.
Wurtz RH, Sommer MA, Paré M, Ferraina S (2001) Signal transformations from cerebral cortex to superior colliculus for the generation of saccades. Vision Res 41:3399–3412.
Zanos TP, Mineault PJ, Pack CC (2011) Removal of spurious correlations between spikes and local field potentials. J Neurophysiol 105:474–486.
Zanos S, Zanos TP, Marmarelis VZ, Ojemann GA, Fetz EE (2012) Relationships between spike-free local field potentials and spike timing in human temporal cortex. J Neurophysiol 107:1808–1821.
Zhao X, Liu M, Cang J (2014) Visual cortex modulates the magnitude but not the selectivity of looming-evoked responses in the superior colliculus of awake mice. Neuron 84:202–213.